Energy Fuels **2010,** *24,* 5773–5780 · DOI:10.1021/ef100817f
Published on Web 09/30/2010

energy&fuels
article

MgO/Al_2O_3 Sorbent for CO_2 Capture

Lei Li,[†,‡] Xia Wen,[†] Xin Fu,[†,‡] Feng Wang,[†] Ning Zhao,[†] Fukui Xiao,[†] Wei Wei,*[,†] and Yuhan Sun*[,†,§]

[†]*State Key Laboratory of Coal Conversion, Institute of Coal Chemistry, Chinese Academy of Sciences, Taiyuan 030001, People's Republic of China,* [‡]*Graduate University of the Chinese Academy of Sciences, Beijing 100049, People's Republic of China, and* [§]*Low Carbon Energy Center, Shanghai Advanced Research Institute, Chinese Academy of Sciences, Shanghai 201203, People's Republic of China*

Received June 22, 2010. Revised Manuscript Received September 15, 2010

The MgO/Al_2O_3 sorbent for CO_2 capture under low temperatures was investigated in a fixed bed. It was found that, with MgO loading of 10 wt %, MgO/Al_2O_3 sorbent showed a maximum CO_2 capture capacity, which originated from the balance of physical adsorption and chemical absorption of the sorbent. The CO_2 capture capacity increased with the water vapor at first and then decreased. Typically, the total CO_2 capture capacities were as high as 0.97 and 1.36 mmol/g, with water vapor concentration of 0 and 13 vol %, respectively, at 60 °C with 13 vol % CO_2. The high CO_2 concentration could be approached by the multistage absorption/desorption cycles, during which the sorbent could be regenerated at 350 °C and maintained stable even after 5 cycles. In addition, a deactivation model was proposed that gave good predictions of the CO_2 breakthrough curves. Results showed that sorption rate parameters obtained in the presence of water vapor were found to be larger than the corresponding values in the absence of water vapor. It was possibly caused by increasing the reactivity of the sorbent prior to the sorption of CO_2 in the presence of water vapor.

1. Introduction

The control of greenhouse gas is arguably the most challenging environmental policy issue facing China and other countries. CO_2 is considered to be the major greenhouse gas contributing to global warming.[1−6] In the current stage, over 85% of world energy demand is supplied by fossil fuels. Roughly, 40% of total CO_2 emissions result from coal-fueled power or heat plants.[7] To reduce the CO_2 emissions, several methods have been developed for CO_2 capture in flue gas, such as wet absorption, adsorption, membrane separation, and cryogenic fractionation. However, these methods need to overcome the limits of cost and energy required to treat the massive flue gas streams from fossil-fuel-fired power plants.[8,9] As a result, CO_2 chemical absorption using dry regenerable solid sorbents has been proposed as an innovative concept for CO_2 removal. The use of solid sorbents containing alkali metal and alkali earth metal for CO_2 absorption was reported; e.g., K_2CO_3 or Na_2CO_3 supported on various supports could be used as the sorbent, which reacted with CO_2 and H_2O to form alkali hydrogen carbonates.[8−18] They provided some important suggestions for the choice of supports. However, CO_2 capture was obtained only in the presence of water vapor over these sorbents.

Recently, alkali earth metal oxides with a better CO_2 uptake and reversibility were developed. Nevertheless, these sorbents, such as CaO and MgO, were applicable at much higher absorption and regeneration temperatures (less than 860 °C).[19−21] The CO_2 sorption capacities over MgO sorbents were also studied at temperatures lower than 150 °C. A summary of CO_2 sorption capacities on different MgO sorbents is reported in Table 1.[22−30]

*To whom correspondence should be addressed. Telephone: +86-351-4049612. Fax: +86-351-4041153. E-mail: weiwei@sxicc.ac.cn (W.W.); yhsun@sxicc.ac.cn (Y.S.).

(1) Mikkelsen, M.; Jørgensen, M.; Krebs, F. C. *Energy Environ. Sci.* **2010**, *3* (1), 43–81.
(2) Soares, J. L.; Oberziner, A. L. B.; José, H. J.; Rodrigues, A. E.; Moreira, R. F. P. M. *Energy Fuels* **2007**, *21* (1), 209–215.
(3) Sun, Y. H. CO_2 capture and chemical utilization. *Proceedings of the 10th International Conference on CO_2 Utilization*; Tianjin, China, May 17−21, 2009; p 21.
(4) Bredesen, R.; Jordal, K.; Bolland, O. *Chem. Eng. Process.* **2004**, *43* (9), 1129–1158.
(5) Xiong, R. T.; Ida, J.; Lin, Y. S. *Chem. Eng. Sci.* **2003**, *58* (29), 4377–4385.
(6) Drage, T. C.; Blackman, J. M.; Pevida, C.; Snape, C. E. *Energy Fuels* **2009**, *23*, 2790–2796.
(7) Carapellucci, R.; Milazzo, A. *Proc. Inst. Mech. Eng., Part A* **2003**, *217* (5), 505–517.
(8) Seo, Y.; Jo, S. H.; Ryu, H. J.; Bae, D. H.; Ryu, C. K.; Yi, C. K. *Korean J. Chem. Eng.* **2007**, *24* (3), 457–460.
(9) Park, Y. C.; Jo, S. H.; Park, K. W.; Park, Y. S.; Yi, C. K. *Korean J. Chem. Eng.* **2009**, *26* (3), 874–878.
(10) Yi, C. K.; Jo, S. H.; Seo, Y.; Lee, J. B.; Ryu, C. K. *Int. J. Greenhouse Gas Control* **2007**, *1* (1), 31–36.
(11) Lee, S. C.; Kim, J. C. *Catal. Surv. Asia* **2007**, *11* (4), 171–185.
(12) Lee, S. C.; Choi, B. Y.; Lee, T. J.; Ryu, C. K.; Ahn, Y. S.; Kim, J. C. *Catal. Today* **2006**, *111* (3−4), 385–390.
(13) Zhao, C. W; Chen, X. P.; Zhao, C. S. *Energy Fuels* **2010**, *24*, 1009–1012.
(14) Hirano, S.; Shigemoto, N.; Yamada, S.; Hayashi, H. *Bull. Chem. Soc. Jpn.* **1995**, *68* (3), 1030–1035.
(15) Hayashi, H.; Taniuchi, J.; Furuyashiki, N.; Sugiyama, S.; Hirano, S.; Shigemoto, N.; Nonaka, T. *Ind. Eng. Chem. Res.* **1998**, *37* (1), 185–191.
(16) Ficicilar, B.; Dogu, T. *Catal. Today* **2006**, *115* (1−4), 274–278.
(17) Park, S. W.; Sung, D. H.; Choi, B. S.; Oh, K. J.; Moon, K. H. *Sep. Sci. Technol.* **2006**, *41* (12), 2665–2684.
(18) Liang, Y.; Harrison, D. P.; Gupta, R. P.; Green, D. A.; McMichael, W. J. *Energy Fuels* **2004**, *18* (2), 569–575.
(19) Abanades, J. C.; Anthony, E. J.; Wang, J. S.; Oakey, J. E. *Environ. Sci. Technol.* **2005**, *39* (8), 2861–2866.
(20) Wang, X. P.; Yu, J. J.; Cheng, J.; Hao, Z. P.; Xu, Z, P. *Environ. Sci. Technol.* **2008**, *42* (2), 614–618.
(21) Yong, Z.; Mata, V.; Rodrigues, A. E. *Sep. Purif. Technol.* **2002**, *26* (2−3), 195–205.
(22) Lee, S. C.; Chae, H. J.; Lee, S. J.; Choi, B. Y.; Yi, C. K.; Lee, J. B.; Ryu, C. K.; Kim, J. C. *Environ. Sci. Technol.* **2008**, *42* (8), 2736–2471.
(23) Ward, S. M.; Braslaw, J.; Gealer, R. L. *Thermochim. Acta* **1983**, *64* (1−2), 107–114.
(24) Choi, S.; Drese, J. H.; Jones, C. W. *ChemSusChem* **2009**, *2* (9), 796–854.
(25) Fu, X.; Zhao, N.; Li, J. P.; Xiao, F. K.; Wei, W.; Sun, Y. H. *Adsorpt. Sci. Technol.* **2009**, *27* (6), 593–601.

Table 1. CO_2 Sorption Capacities over MgO Sorbents from the Literature

material	sorption temperature (°C)	CO_2 partial pressure (bar)[a]	total capacity (mmol/g)	method[b]	reference
MgO	60	0.01		GC	22
MgO	60	0.01[c]	1.05	GC	22
MgO	0	0.2	0.64	TGA	23 and 24
MgO	100	0.2	0.43	TGA	23 and 24
MgO/MCM-41	25	1	1.06	TGA	25
mesoporous MgO	25	1	1.82	TGA	26
mesoporous MgO	100	1	2.27	TGA	26
non-porous MgO	25	1	0.03	TGA	26
Mg−Al−CO_3 (LDH)[d]	100	1	0.23	TGA	27
EXM911[e]	20	1	0.13	TGA	28
EXM696[f]	20	1	0.25	TGA	28
MgO−ZrO_2[g]	30	1	1.15	GC	29
MgO	150	1	0.63	TGA	30
MgO−ZrO_2[g]	150	1	1.01	TGA	30

[a] Total pressure = 1 bar. [b] GC, gas chromatography; TGA, thermogravimetric analysis. [c] In the presence of 9 vol % H_2O. [d] LDH = layered double hydroxide. [e] EXM911 = commercial hydrotalcite-like compounds (Al_2O_3, 22.4 wt %; MgO, 31.7 wt %). [f] EXM696 = commercial hydrotalcite-like compounds (Al_2O_3, 20.8 wt %; MgO, 33.8 wt %). [g] MgO−ZrO_2 (Mg/Zr molar ratio of 0.5).

The sorption capacities of CO_2 on this material were not high, and most of these studies quantified CO_2 capture capacities by thermogravimetric analysis (TGA), which cannot differentiate between CO_2 and H_2O. Furthermore, It is unclear whether these sorbents can perform at the reported level under practical conditions, where the flue gas of the coal power plant contains 8−17 vol % water vapor and 10−15 vol % CO_2.[14,15,31,32] A previous study revealed that MgO/Al_2O_3 sorbent showed a better performance for CO_2 capturing at low temperature in the absence of water vapor, which might be attributed to both physical adsorption and chemical absorption.[33] However, related absorption dynamics and the water vapor effect were not well-established. Thus, CO_2 absorption over MgO/Al_2O_3 sorbent was carried out in a fixed-bed reactor to investigate the effect of the capture and regeneration operation in the present work. Moreover, the deactivation model (DM), as a simplified model, had been successfully used for the prediction of the breakthrough curves for CO_2 sorption on solid adsorbent in the fixed bed, assuming that the formation of a dense product layer over the surface of the sorbent changed the number of active sites, causing a drop in the sorption rate.[16,17,20,34,35] In this study, the sorption and deactivation were evaluated by the DM via the analysis of the experimental breakthrough data using a nonlinear least-squares technique.

2. Experimental Section

2.1. Material Preparation. Five MgO/Al_2O_3 samples with different MgO loadings (0, 5, 10, 20, and 30 wt %) were prepared by impregnating a certain amount of calcined γ-Al_2O_3 support (supplied by the China Research Institute of Daily Chemical Industry) with an aqueous solution of $Mg(NO_3)_2 \cdot 6H_2O$ (supplied by the Tian Jin Bodi Chemical Holding Co., Ltd.). The samples were stirred for 12 h at room temperature, dried at 110 °C for 12 h, and calcined in a furnace under N_2 flow (20 mL/min) at 550 °C for 6 h.

Table 2. Texture Properties of Different Samples

MgO/Al_2O_3 (wt %)	BET surface area (m^2/g)	pore space (cm^3/g)	bulk density (g/cm^3)	average pore diameter (nm)	crushing strength (N/cm^2)
0	253.47	0.79	0.33	18.1	716
5	226.55	0.70	0.35	18.2	825
10	200.91	0.60	0.38	17.3	935
20	185.16	0.56	0.36	17.9	978
30	160.21	0.53	0.36	18.2	998

2.2. Material Characterization. X-ray diffraction (XRD) experiments were performed in the 2θ range of 10−80° using Cu Kα radiation at room temperature (Rigaku D/max-A X-ray diffractometer). The surface area of catalysts was determined with the Brunauer−Emmett−Teller (BET) method using N_2 on a Micromeritics ASAP-2020 instrument. The pore volume and pore size distribution were obtained with the Bopp−Jancso−Heinzinger method from the absorption isotherm. The crushing strength was measured by the digital crushing strength tester (Jiangyan Global Instrument Factory KC-3C), which was a dynamometer measuring the force progressively applied to the solid object during the advancement of a piston. The applied force increases until the solid breaks and collapses into small pieces and eventually powder. The corresponding value of the collapsing force is defined as the crushing strength. The detailed properties of different samples are shown in Table 2.

Temperature-programmed desorption (TPD) of CO_2 was performed in a quartz microreactor. A total of 0.1 g (40−60 mesh) of sample was first heated in helium at 500 °C for 4 h. CO_2 was introduced to the sample after it was cooled to room temperature (30 °C). To remove weakly adsorbed CO_2, the sample was swept using flowing argon at room temperature. The TPD of CO_2 was performed at a heat of 10 °C/min under argon flow of 50 mL/min, and CO_2 desorbed was detected by a BALZA Q-Mass spectrometer.

The structure of CO_2 chemisorbed over MgO/Al_2O_3 sorbent was determined by *in situ* Fourier transform infrared (FTIR) spectroscopy. The sorbent was pressed into a 15 mm self-supporting wafer and mounted into a quartz cell. In the case of CO_2 adsorption, the sample was pretreated under vacuum at 400 °C for 4 h. Data were collected using a Nicolet 470 FTIR spectrometer operating at a resolution of 4 cm^{-1} after CO_2

(26) Bhagiyalakshmi, M.; Lee, J. Y.; Jang, H. T. *Int. J. Greenhouse Gas Control* **2010**, *4* (1), 51–56.
(27) Ram Reddy, M. K.; Xu, Z. P.; Lu, G. Q.; Diniz da Costa, J. C. *Ind. Eng. Chem. Res.* **2006**, *45* (22), 7504–7509.
(28) Yong, Z.; Mata, V.; Rodrigues, A. E. *Ind. Eng. Chem. Res.* **2001**, *40* (1), 204–209.
(29) Liu, S. G.; Zhang, X. L.; Li, J. P.; Zhao, N.; Wei, W.; Sun, Y. H. *Catal. Commun.* **2008**, *9* (7), 1527–1532.
(30) Li, B.; Wen, X.; Zhao, N.; Wang, X. Z.; Wei, W.; Sun, Y, H.; Ren, Z. H.; Wang, Z. J. *J. Fuel Chem. Technol.* **2010**, *38* (4), 473–477.
(31) Xu, X. C.; Song, C. S.; Miller, B. G.; Scaroni, A. W. *Ind. Eng. Chem. Res.* **2005**, *44* (21), 8113–8119.
(32) Park, J. H.; Beum, H. T.; Kim, J. N.; Cho, S. H. *Ind. Eng. Chem. Res.* **2002**, *41* (16), 4122–4131.
(33) Fu, X.; Wu, D. D.; Li., J. P.; Zhao, N.; Wei, W.; Sun, Y. H. *Prepr. Pap.—Am. Chem. Soc., Div. Fuel Chem.* **2008**, *53* (1), 234–235.
(34) Hwang, K. S.; Han, L.; Park, D. W.; Oh, K. J.; Kim, S. S.; Park, S. W. *Korean J. Chem. Eng.* **2010**, *27* (1), 241–248.
(35) Hwang, K. S.; Son, Y. S.; Park, S. W.; Park, D. W.; Oh, K. J.; Kim, S. S. *Sep. Sci. Technol.* **2010**, *45* (1), 85–93.

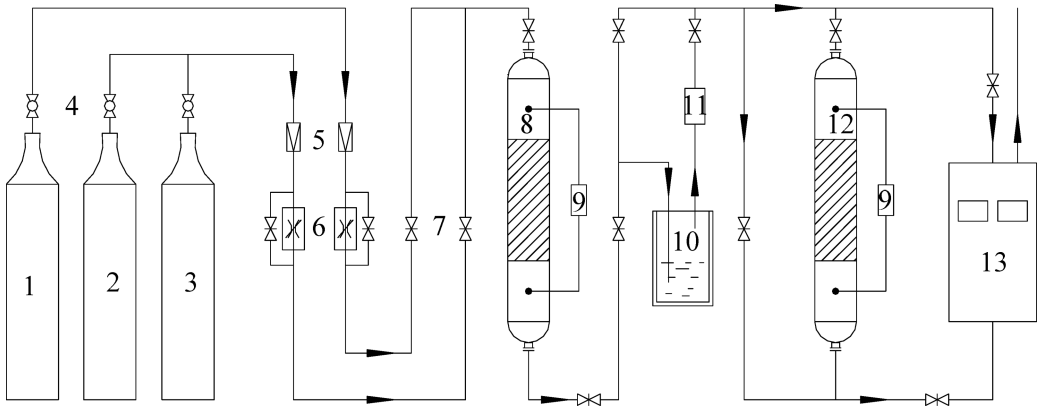

Figure 1. Flowchart of the fixed-bed experimental apparatus: (1) CO_2, (2) N_2, (3) argon, (4) ball valve, (5) redactor, (6) mass flow controllers, (7) gate valve, (8) preheater, (9) temperature controller, (10) bubbler, (11) water vapor analyzer, (12) absorption column, and (13) CO_2 analyzer.

adsorption at room temperature (30 °C) and sequential evacuation at 150, 300, and 450 °C.

2.3. Apparatus and Operation Description. Figure 1 gives the flowchart of the fixed-bed experimental apparatus. It mainly consists of three parts, including a gas injection part, fixed-bed absorption system, and gas concentration analysis system. Typically, 7.2 g (20−40 mesh) of MgO/Al_2O_3 sorbent was packed into a stainless-steel absorption column (16 mm in diameter and 250 mm in length) and supported by quartz wool from both sides. The sorbent was pretreated at 350 °C for 4 h with argon flowing at 50 mL/min. After cooling to the absorption temperature, the simulated flue gas (a composition of CO_2 and N_2) was introduced into the fixed-bed reactor. In this study, contaminants in flue gas, such as SO_x and NO_x, were neglected because they were practically reduced to low levels prior to CO_2 capture via desulfurization and denitrification processes. The bed temperature was controlled by a temperature controller and measured by thermocouples. Besides, the water vapor (8−17 vol % or higher in flue gas[14,15,31]) was simulated by passing a mixed gas of CO_2 and N_2 through a temperature-controlled gas bubbler, and the feed pipeline was heated to avoid H_2O condensation. The water vapor of the volume fraction was analyzed by the relative humidity analyzer (Vaisala, Finland). The flow was monitored by the mass flow controllers, which were placed at the inlet of the column. CO_2 in the outlet was monitored online by a gas analyzer (Vaisala, Finland) every 20 s.

It should be mentioned that the pressure drop of absorber was negligible because of low superficial velocity and thin bed height. As a result, the flow rates at the inlet and outlet of the fixed-bed absorber were assumed to be the same and the bed pressure remained constant for each experimental condition. According to the mass balance of CO_2, the total and breakthrough capacities could be determined by[36]

$$q = \frac{Qt_sC_0}{22.4W} \quad (1)$$

$$t_s = \int_0^t (1 - \frac{C_t}{C_0})\mathrm{d}t \quad (2)$$

where t_s is the mean residence time (min), C_t is the outlet concentration of CO_2, C_0 is the CO_2 concentration in the feed, q is the equilibrium absorption capacity of CO_2 (mmol/g), t is the absorption time (min), Q is the feed volumetric flow rate (mL/min) at standard temperature and pressure (1 bar and 0 °C), and W is the mass of the sorbent (g). In this work, it was a long enough time (t = 60 min) to saturate the sorbent. The total capacity was calculated by eqs 1 and 2, while the breakthrough capacity was calculated by eqs 1 and 2 when the effluent CO_2 concentration reached 5% of its feed concentration. The breakthrough curves were reflected by the gradual increase of the C_{out}/C_{in} ratio (C_{out} and C_{in} refer to the CO_2 concentrations in the outlet and inlet flue gas, respectively). All of the experimental conditions and results are listed in Table 3, and the run numbers in the following text refer to those listed in the table.

3. Results and Discussion

3.1. Material Structure. The solid sorbent with different amounts of MgO showed the diffraction peaks at 2θ of 19.44°, 34.59°, 39.47°, 45.84°, and 67.00° and at 2θ of 42.99°, 62.34°, 74.65°, and 78.28° assigned to γ-Al_2O_3 and MgO, respectively (Figure 2). Clearly, no diffraction of MgO was observed until the MgO loading reached 20 wt %, which indicated that MgO was highly dispersed on the internal surfaces of the mesopores in the samples. However, peaks corresponding to MgO appeared at MgO loadings over 20 wt %, probably as a result of the presence of MgO on the external surface of the support. Furthermore, the increase of the MgO content led to a decrease in the surface area and pore volume but an increase in the crushing strength. Nevertheless, no significant change for the average pore diameter was observed (Table 2).

Figure 3 illustrates the CO_2−TPD profiles of 10 wt % MgO/Al_2O_3. Three desorption peaks were observed at 130, 200, and 480 °C, respectively, indicating the presence of three kinds of basic sites. The absorbed species formed from CO_2 on the sorbent can be identified by *in situ* IR spectra (Figure 4). IR spectra revealed the C−OH bending vibration at 1220 cm^{-1} and the O−C−O stretching vibration at 1650 cm^{-1} of bicarbonate species. Moreover, the bands at 1420, 1506, 1574, and 1591 cm^{-1} ascribed to unidentate carbonate species as well as the bands at 1380 and 1708 cm^{-1} attributed to bidentate carbonate species were also detected.[37−39] After evacuation at 150 °C, the bicarbonate species disappeared, while unidentate and bidentate carbonates remained even after evacuation at 300 °C. However, the band at 1708 cm^{-1} attributed to bidentate carbonate species was not observed on curves b and c of Figure 4, which might be because it was a weaker band.[39] It was also found that only unidentate carbonates species were detected after evacuation at 450 °C. As a result, the three desorption peaks in the CO_2−TPD profile might

(36) Chang, H.; Wu, Z. X. *Ind. Eng. Chem. Res.* **2009**, *48* (9), 4466–4473.

(37) Di Cosimo, J. I.; Díez, V. K.; Xu, M.; Iglesia, E.; Apesteguía, C. R. *J. Catal.* **1998**, *178* (2), 499–510.

(38) Prescott, H. A.; Li, Z. J.; Kemnitz, E.; Trunschke, A.; Deutsch, J.; Lieske, H.; Auroux, A. *J. Catal.* **2005**, *234* (1), 119–130.

(39) Lercher, J. A.; Colombier, C.; Noller, H. *J. Chem. Soc., Faraday Trans. 1* **1984**, *80*, 949–959.

Table 3. Experimental Conditions and Results[a]

run	sorbent (wt %)	temperature (°C)	flow (mL/min)	CO_2 (vol %)	H_2O (vol %)	total capacity (mmol/g)	breakthrough capacity (mmol/g)	k_0 (mL min^{-1} g^{-1})	k_d (min^{-1})	R^2
1	0	30	80	8	0	0.59	0.44	68.24	0.46	0.9997
2	5	30	80	8	0	0.61	0.46	70.65	0.46	0.9992
3	20	30	80	8	0	0.62	0.43	72.27	0.48	0.9966
4	30	30	80	8	0	0.57	0.41	68.86	0.45	0.9994
5	10	30	80	8	0	0.69	0.55	79.05	0.43	0.9972
6	10	50	80	8	0	0.67	0.42	68.76	0.45	0.9862
7	10	70	80	8	0	0.63	0.39	66.57	0.46	0.9849
8	10	110	80	8	0	0.56	0.32	57.56	0.47	0.9812
9	10	150	80	8	0	0.49	0.26	47.92	0.46	0.9804
10	10	30	60	8	0	0.71	0.59	78.23	0.42	0.9981
11	10	30	100	8	0	0.66	0.46	74.55	0.45	0.9985
12	10	30	120	8	0	0.63	0.41	75.40	0.49	0.9993
13	10	60	80	8	0	0.67	0.46	65.55	0.41	0.9957
14	10	60	80	10	0	0.77	0.56	65.64	0.43	0.9989
15	10	60	80	13	0	0.97	0.66	66.75	0.46	0.9973
16	10	60	80	13	8	1.19	0.88	86.78	0.48	0.9963
17	10	60	80	13	11	1.28	0.97	93.50	0.48	0.9967
18	10	60	80	13	13	1.36	1.07	94.79	0.44	0.9988
19	10	60	80	13	15	1.09	0.77	78.51	0.49	0.9958

[a] Sorbent, MgO/Al_2O_3; temperature, absorption temperature; k_0, initial sorption rate constant; k_d, deactivation rate constant; R^2, correlation coefficient; pressure, 1 bar; balance gas, N_2; mass of MgO/Al_2O_3 sorbent, 7.2 g.

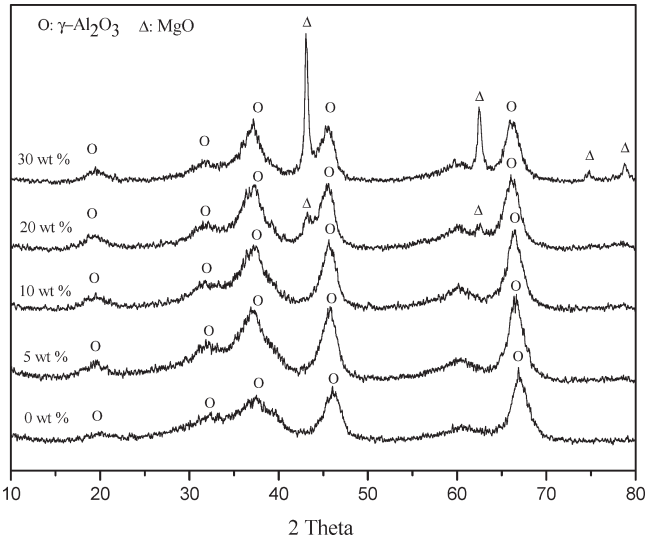

Figure 2. XRD patterns of different samples.

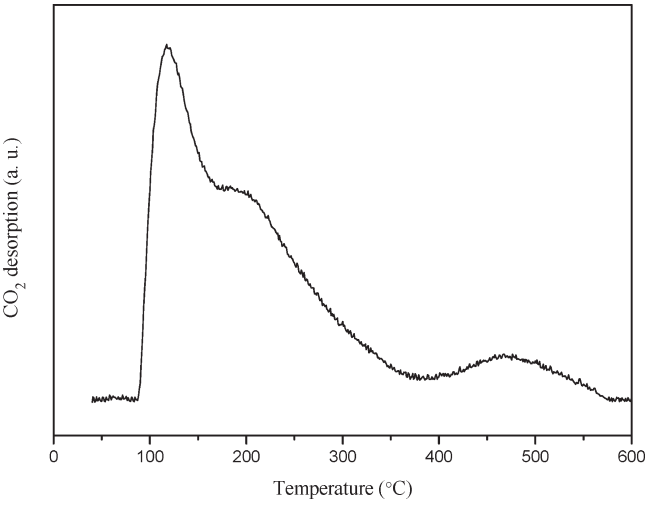

Figure 3. CO_2−TPD profiles of MgO/Al_2O_3 (10 wt %) sorbent.

correspond to bicarbonate, bidentate, and unidentate species, respectively.

3.2. Effect of MgO Loadings. Runs 1−5 (Table 3) show the effect of MgO loadings on the total capacity of CO_2 absorption at 30 °C. It was found that, upon increasing of MgO loadings, the amount of adsorbed CO_2 reached the maximum at 10 wt % MgO, which might originate from the balance of physical adsorption (high BET surface area) and chemical absorption (high MgO loading) of the sorbent. Thus, the sorbent loading 10 wt % MgO was selected for further investigations.

3.3. Effect of the Temperature. To investigate the effect of the temperature on the capacity of CO_2 absorption over the sorbent, the experiments were carried out in the range of temperatures from 30−150 °C. Figure 5 shows the total CO_2 capture capacity over MgO/Al_2O_3 and γ-Al_2O_3 sorbents as a function of the temperature. Clearly, the CO_2 capture capacity decreased as the temperature increased because both physical adsorption and chemical absorption were exothermic processes.[40−42] Moreover, it was observed that MgO/Al_2O_3 had a higher CO_2 absorption capacity than γ-Al_2O_3, which might be because of the chemical interaction of CO_2 and MgO of the MgO/Al_2O_3 sorbent. In other words, the introduction of MgO onto γ-Al_2O_3 could improve the selective capture toward CO_2. The total capacity and the breakthrough capacity of CO_2 on MgO/Al_2O_3 sorbent at different temperatures were calculated by eqs 1 and 2. The results (runs 5−9 in Table 3) indicate that low temperature is favorable for CO_2 capture over the MgO/Al_2O_3 sorbent.

3.4. Effect of the Flow Rate. To investigate the effect of the flow rate on the kinetics, the breakthrough curves of CO_2 were measured in the range of the gaseous flow rate of 60−120 mL/min. Figure 6 gives the breakthrough curves of CO_2 against the absorption time at various flow rates, and both total and breakthrough capacities of CO_2 are listed in

(40) Ruthven, D. M. *Principles of Adsorption and Adsorption Processes*; John Wiley and Sons, Inc.: New York, 1984.

(41) Atkins, P. W. *Physical Chemistry*; Oxford University Press: Oxford, U.K., 1990.

(42) Voyutsky, S. *Colloid Chemistry*; MIR Publishers: Moscow, Russia, 1978.

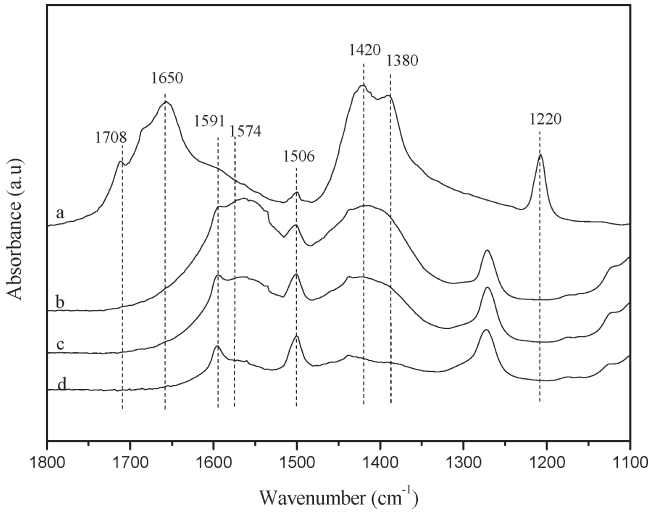

Figure 4. IR spectra of CO_2 adsorbed over MgO/Al_2O_3 sorbent upon increasing evacuation temperatures: (a) 30 °C, (b) 150 °C, (c) 300 °C, and (d) 450 °C.

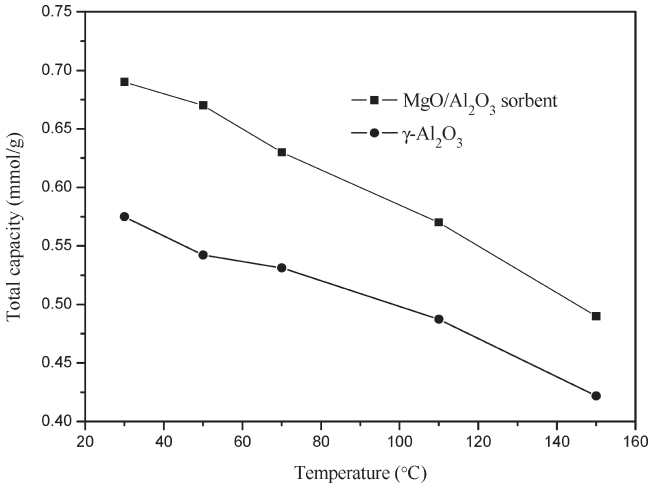

Figure 5. Effect of the temperature on the total capacity of CO_2 over MgO/Al_2O_3 and γ-Al_2O_3 sorbents. Pressure, 1 bar; flow rate, 80 mL/min; feed gas, 8 vol % CO_2 and 92 vol % N_2; amount of MgO/Al_2O_3 sorbent, 7.2 g.

Table 3 (runs 5 and 10−12). A shift of breakthrough curves to shorter time was observed at a higher flow rate of the gas, which suggested that the absorbed capacity of CO_2 decreased as the space time of the gaseous mixtures in the fixed bed decreased.[10,17,34,35]

3.5. Effect of the Water Vapor on the Breakthrough Curve of CO_2. Figure 7 shows the total CO_2 capture capacity over MgO/Al_2O_3 and γ-Al_2O_3 sorbents at 45 °C as a function of the water vapor concentration. It was clear that, for the MgO/Al_2O_3 sorbent, CO_2 absorption capacity increased sharply in the presence of water vapor, which indicated that water vapor could promote the absorption of CO_2. This was possibly caused by either the increase of CO_2 sorption capacity with the CO_2 dissolving in water or the chemical interaction between CO_2 and MgO in the presence of water. In the absence of water, the main reaction between CO_2 and MgO was the formation carbonate, while with the introduction of

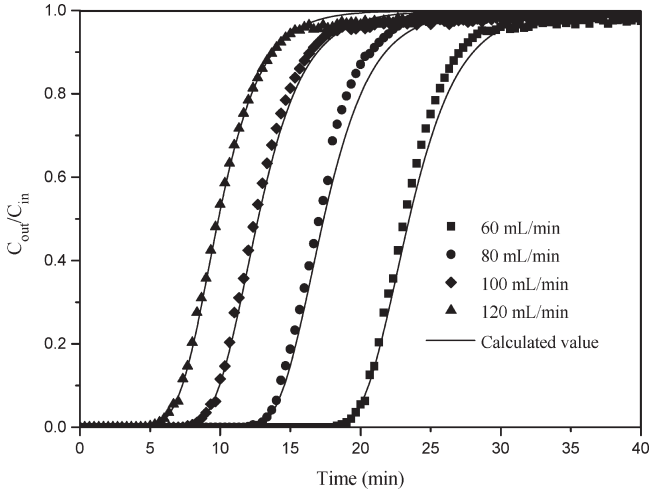

Figure 6. Breakthrough curves of CO_2 against the absorption time at various flow rates. Absorption temperature, 30 °C; pressure, 1 bar; feed gas, 8 vol % CO_2 and 92 vol % N_2; amount of MgO/Al_2O_3 sorbent, 7.2 g.

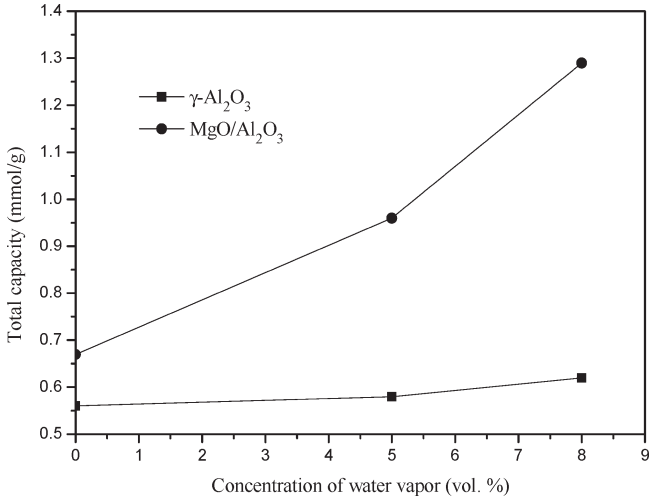

Figure 7. Total capacity of CO_2 over MgO/Al_2O_3 and γ-Al_2O_3 sorbents at 45 °C as a function of the water vapor concentration. Absorption temperature, 45 °C; pressure, 1 bar; flow rate, 80 mL/min; feed gas, 8 vol % CO_2; balance gas, N_2; amount of sorbent, 7.2 g.

water vapor, the carbonate could further react with CO_2 and H_2O to form hydrous carbonates.[43] While for γ-Al_2O_3, the capacity of CO_2 absorption hardly changed in the presence of water vapor, which suggested that the dissolution of CO_2 in the adsorbed water was very little. Thus, the increase in the CO_2 absorption capacity for MgO/Al_2O_3 with the introduction of water vapor might originate from the formation of hydrous carbonates.

In the presence of water vapor, the absorption temperature should be above the dew point of the feed gas stream to prevent water vapor condensation. In this study, the temperature (60 °C) was chosen to investigate the effect of water vapor on the CO_2 capture capacity. As shown in Figure 8, at low water vapor concentration, the breakthrough curves of CO_2 significantly shifted to the right. The data of CO_2 capture capacity are listed in Table 3 (runs 15−19). Clearly, the total CO_2 absorption capacity was 0.97, 1.19, and 1.36 mmol/g for the feed with the water vapor concentrations of 0, 8, and 13 vol %, respectively. However, when the concentration increased to 15 vol %, the CO_2 absorption capacity decreased. Interestingly,

(43) Vágvölgyi, V.; Hales, M.; Frost, R. L.; Locke, A.; Kristóf, J.; Horváth, E. *J. Therm. Anal. Calorim.* **2008**, *94* (2), 523–528.

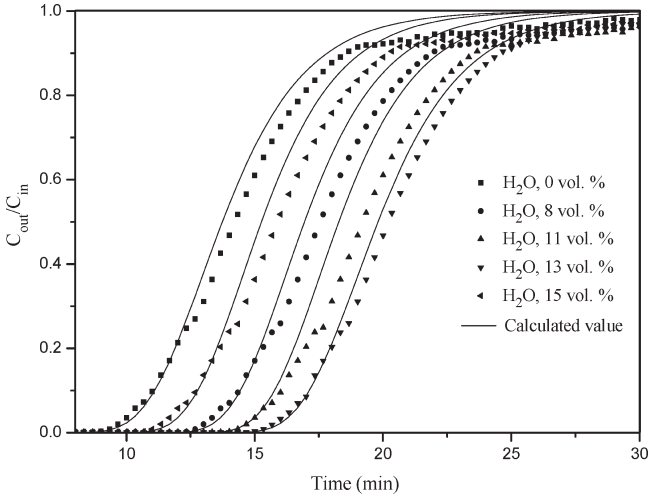

Figure 8. Breakthrough curves of CO_2 on MgO/Al_2O_3 sorbent at different concentrations of water vapor. Absorption temperature, 60 °C; pressure, 1 bar; flow rate, 80 mL/min; feed gas, 13 vol % CO_2; balance gas, N_2; amount of MgO/Al_2O_3 sorbent, 7.2 g.

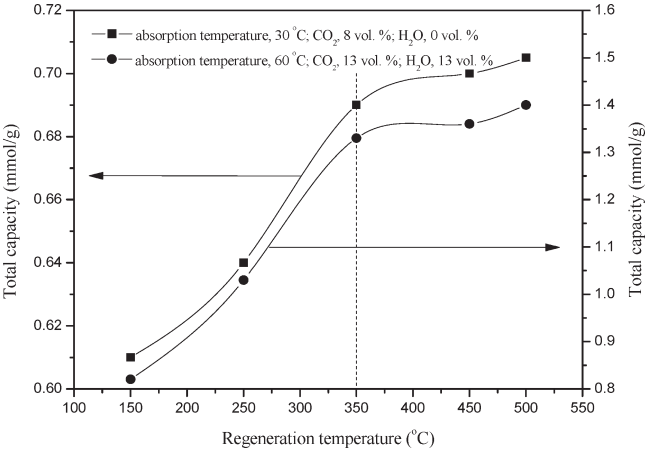

Figure 9. Effect of the regeneration temperature on the absorption capability of CO_2 over MgO/Al_2O_3 sorbent in the presence and absence of water vapor. Pressure, 1 bar; flow rate, 80 mL/min; balance gas, N_2; amount of MgO/Al_2O_3 sorbent, 7.2 g.

when the feed concentration of water vapor was lower than that of CO_2, the CO_2 sorption capacity increased rapidly with the increase of the water vapor concentration. It was possibly caused by increasing the reactivity of the sorbent prior to the sorption of CO_2 in the presence of small amounts of water vapor. For the feed concentration of water vapor higher than that of CO_2, the CO_2 absorption capacity decreased upon the increase of the water vapor concentration. This might be due to the shrinkage of pore mouths in the presence of excessive water vapor. The sorption of H_2O and CO_2 near the pore mouths could cause an additional diffusion resistance for the transportation of CO_2 to the active surface of the sorbent, which was similar to the result of absorption CO_2 over the hydrotalcite in the presence of excess water vapor.[16]

3.6. Effect of the Regeneration Temperature. Figure 9 shows the effect of the regeneration temperature on the absorption capability of CO_2 over the MgO/Al_2O_3 sorbent in the presence and absence of water vapor. The saturated sorbents (absorption of CO_2 at 60 °C with water vapor and absorption of CO_2 at 30 °C without water vapor) were exposed to the temperatures of 150, 250, 350, 450, and 500 °C in argon for desorption for 4 h followed by re-absorption. It can be seen that, with the desorption temperature lower than 350 °C, the CO_2 absorption capacity increased upon increasing the regeneration temperature, indicating that the carbonate was not desorbed completely. At the regeneration temperature higher than 350 °C, the CO_2 absorption capacity hardly increased with the increase in the regeneration temperature. Therefore, the regeneration temperature of 350 °C might be suitable for sorbent recycle. From a practical point of view, it was desirable that the sorbent could be regenerated by the hot flue gas (around 400−600 °C[5,20]) from a coal burner, which made the CO_2 capture process more feasible and economic.

3.7. Stability of the MgO/Al_2O_3 Sorbent in Multiple Cycles. Figure 10 shows the CO_2 concentration change during the absorption/desorption cycle over the MgO/Al_2O_3 sorbent. The absorption/desorption cycle operation consisted of three basic steps: absorption, desorption, and purge. The absorption/desorption cycle was carried out at 45 °C in the absence and presence of water vapor, respectively. CO_2 was detected, and the concentration slowly increased to the feed concentration and did not change anymore, which illustrated that the

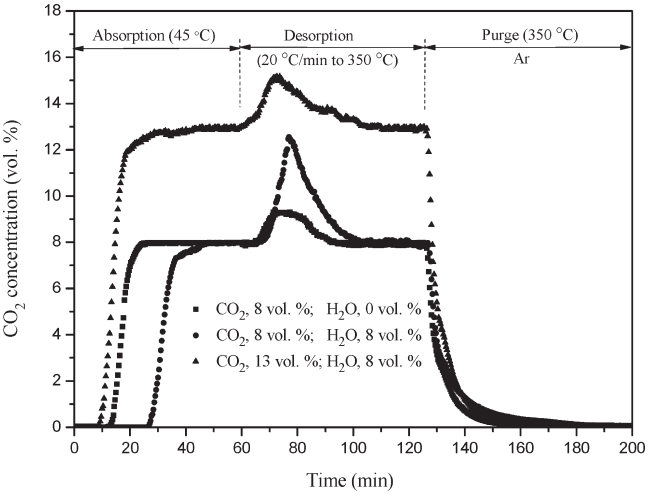

Figure 10. CO_2 concentration change during the absorption/desorption cycle. Absorption temperature, 45 °C; pressure, 1 bar; flow rate, 80 mL/min; balance gas, N_2; amount of MgO/Al_2O_3 sorbent, 7.2 g.

absorption/desorption process reached equilibrium. In the temperature swing adsorption (TSA) process, desorption was carried out by increasing the bed temperature from 45 to 350 °C with the heating rate of 20 °C/min.

To shorten the desorption time and avoid contamination, the feed gas were used in the desorption process. A high CO_2 effluent concentration was obtained at elevated temperatures during the desorption step. It was also found that the desorption concentration of CO_2 in the presence of water was higher than that for dry feed gas, which confirmed that the water vapor had a positive effect on the absorption of CO_2. As seen from Figure 10, during the desorption step, 13 vol % CO_2 was obtained after heating the sorbent saturated by 8 vol % CO_2 and 8 vol % H_2O at 45 °C. Afterward, 13 vol % CO_2 was reabsorbed by the fresh sorbent, and then the saturated sorbent was heated again in the feed gas. As a result, the concentration of CO_2 obtained in the desorption process of the flue gas increased from 8 to 16 vol %, which meant that a higher concentration of CO_2 could be obtained by the multistage absorption/desorption cycles. In the purge process, the sorbent was carried out at 350 °C in argon for 40 min. It

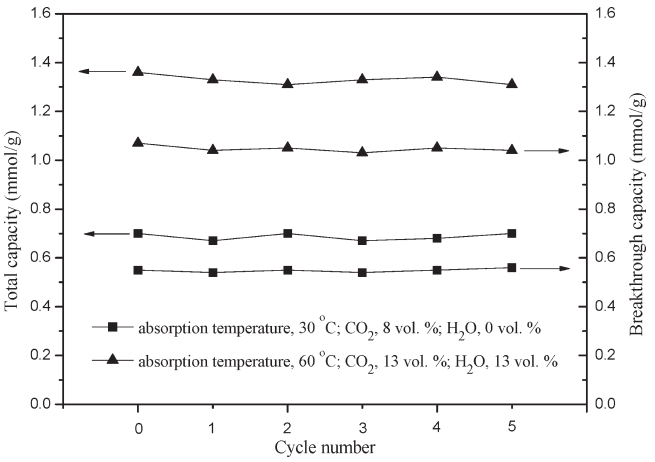

Figure 11. Total and breakthrough capacities of CO_2 over the MgO/Al_2O_3 sorbent in the presence and absence of water vapor for multiple absorption/desorption cycles. Pressure, 1 bar; flow rate, 80 mL/min; balance gas, N_2; regeneration temperature, 350 °C; amount of MgO/Al_2O_3 sorbent, 7.2 g.

revealed that the MgO/Al_2O_3 sorbent could be completely regenerated at this stage.

For practical application, the sorbent should not only possess high capacity and high selectivity but also show a stable performance for multiple absorption/desorption cycles. As shown in Figure 11, CO_2 absorption capacity (total and breakthrough capacities) hardly changed after 5 cycles, indicating that the sorbent was stable.

3.8. Breakthrough Analysis using the Deactivation Model. The sorption of CO_2 on MgO/Al_2O_3 appears not to be a simple absorption process. Rather, these sorption processes may be described as chemisorption or gas−solid non-catalytic reactions, including CO_2 diffusion into the surface and pores, reaction with the active sites, and formation of a product layer of carbonate or hydrous carbonates on the surface. With the sorption proceeding, it will be more and more difficult for CO_2 to diffuse into innerpores/surface or penetrate the product layer to be adsorbed, which seems that the adsorbent is gradually deactivated. A lot of models, such as grain and pore models, were proposed in the literature to describe the conversion−time relations in such gas−solid reactions. Those models contained a large number of variables related to the pore structure, the product layer, and pore diffusion resistances, as well as the surface sorption rate parameters.[16,20] The relevant gas−solid sorption process could also be described with the deactivation model (DM), which had already been successfully used for the prediction of the breakthrough curves for CO_2 sorption on solid adsorbent,[16,17,20,34,35] as well as the sorption of SO_2 and H_2S over various solid materials.[44−46]

According to this model, an activity term α is introduced into the rate expression to represent the deactivation because of a decrease of the active site concentration, the textural changes, etc. The rate of decrease of the activity of the solid reactant is also expected to be proportional to the activity itself and also to the concentration of the absorbing gas. Considering the pseudo-steady-state assumption and neglecting the axial dispersion term, the species conservation equation for the concentration of CO_2 in the fixed bed and the equation for the rate of activity change of the solid reactant with respect to time were described as eqs 3 and 4[16,17,44]

$$-Q\frac{dC_t}{dW} - k_0 C_t \alpha = 0 \quad (3)$$

$$-\frac{d\alpha}{dt} = k_d C_t{}^n \alpha^m \quad (4)$$

where C_t is the CO_2 concentration in the outlet gases, α is the activity of the sorbent, k_0 is the initial sorption rate constant (mL min^{-1} g^{-1}), k_d is the deactivation rate constant (min^{-1}), W is the sorbent mass (g), t is the absorption time (min), and Q is the feed volumetric flow rate (mL/min). For the concentration-independent deactivation, the value of n is equal to 0. More realistically, the deactivation rate is expected to depend upon the concentration of the adsorbing gas. Considering a first-order dependence of the deactivation rate on the concentration of the adsorbing gas ($n = 1$) and also on the activity itself ($m = 1$), the solution of this model gives the following approximate equation for the breakthrough curves:[16,17,20,34,35,44−47]

$$\frac{C_t}{C_0} = \exp\left[\frac{\{1-\exp[(k_0 W/Q)(1-\exp(-k_d t))]\}}{[1-\exp(-k_d t)]}\exp(-k_d t)\right] \quad (5)$$

The breakthrough curves for the deactivation model with two parameters calculated from the concentration profiles using eq 5 are shown in Figures 6 and 8. The initial sorption rate constant k_0 and the deactivation rate constant k_d values obtained by the nonlinear regression analysis of eq 5 are listed in Table 3. The regression seemed very good, with the correlation coefficient R^2 being more than 0.98 in all cases.

Runs 1−5 (Table 3) were conducted to study the effect of MgO loadings on the capacity of CO_2. The results were calculated by the DM based on the experimental data. The constant k_0 of 10 wt % MgO was larger than other samples, being consistent with its highest sorption capacity for CO_2. It confirmed that the balance of physical adsorption (high BET surface area) and chemical absorption (high MgO loading) of the sorbent had a positive effect on the absorption of CO_2. The results calculated from the effect of the temperature on the sorption kinetics are listed in Table 3 (runs 5−9). A steady decrease was observed in the sorption rate constant and an increase in deactivation rate as the temperature increased, which was in accordance with the sorption capacity for CO_2.

To test the validity of the model assumption of neglecting interparticle transport effects, CO_2 sorption experiments were investigated at different flow rates. The calculated curves using eq 5 are shown in Figure 6 as solid lines. As expected, the breakthrough curves shifted to shorter times with an increase in the gas flow rate. As shown in Table 3 (runs 5 and 10−12), the regression analysis of these data showed that both the initial sorption rate constant k_0 and the deactivation rate constant k_d did not have significant changes in the flow rate range. To determine the independence of the sorption parameters on the feed concentration of CO_2, the experiments were carried out with CO_2 input concentrations ranging from 8 to 13 vol %

(44) Yasyerli, S.; Dogu, G.; Ar, I.; Dogu, T. *Ind. Eng. Chem. Res.* **2001**, *40* (23), 5206–5214.
(45) Ozaydin, Z.; Yasyerli, S.; Dogu, G. *Ind. Eng. Chem. Res.* **2008**, *47* (4), 1035–1042.
(46) Kopaç, T.; Kocabaş, S. *Chem. Eng. Commun.* **2003**, *190* (5−8), 1041–1054.
(47) Yaşyerli, S.; Ar, I.; Doğu, G.; Doğu, T. *Chem. Eng. Process.* **2002**, *41* (9), 785–792.

at 60 °C under a flow rate of 80 mL/min (runs 13−15 in Table 3). It indicated that the rate constants k_0 and k_d did not show significant changes in this concentration range.

The initial sorption rate constant k_0 and the deactivation rate constant k_d derived from the data at different water vapor concentrations are listed in Table 3 (runs 15−19), and calculated curves using eq 5 are shown in Figure 8 (solid lines). Although the presence of small amounts of water vapor had a positive effect on the total CO_2 capture capacity, the sorption rate was found to decrease in the presence of excess water vapor. It was similar to the result of absorption of CO_2 onto hydrotalcite with and without water vapor, respectively.[16]

4. Conclusions

The MgO/Al_2O_3 sorbent was found to be an attractive sorbent for low-temperature CO_2 removal, in both the absence and presence of water vapor. When MgO loading reached 10 wt %, the MgO/Al_2O_3 sorbent showed a maximum CO_2 capture capacity. The presence of small amounts of water vapor had a positive effect on the total CO_2 capture capacity. Typically, the total CO_2 capture capacities were as high as 0.97 and 1.36 mmol/g with the water vapor concentration of 0 and 13 vol %, respectively, at 60 °C with 13 vol % CO_2, which are higher than many MgO materials reported before at low temperatures. The high CO_2 concentration could be approached by the multi-stage absorption/desorption cycles, during which the sorbent could be regenerated at 350 °C. Furthermore, the sorbent after CO_2 absorption showed bicarbonate, bidentate, and unidentate species by FTIR analyses. The deactivation model was employed to describe the CO_2 breakthrough curves of the sorbent in the fixed-bed reactor.

Acknowledgment. This work was supported by Lu'an Group, the Knowledge Innovation Programme of the Chinese Academy of Science (2007YQNRC07).